RSC Advances

PAPER

View Article Online
View Journal | View Issue

Cite this: *RSC Adv.*, 2026, **16**, 7717

Fabrication of a zein-phloretin complex and nanoparticles: interaction mechanism and characterization

Siyang Chen,[a] Jinhui Jia,[a] Jian Du,[b] Ningbo Qin *[a] and Xiaodong Xia *[ac]

Due to its capacity to form complexes with polyphenols and to self-assemble as nanoparticles, zein could be utilized as an excellent carrier for polyphenols. The objective of this study was to examine the interaction between zein and phloretin (PHL) through multispectral analysis and molecular docking, and to prepare and characterize PHL-loaded zein nanoparticles. Spectral analysis and docking data confirmed that the binding process of the zein-PHL complex is mainly influenced by hydrogen bonding and van der Waals forces, and hydrophobic interaction was auxiliary, with static quenching as the primary fluorescence quenching mechanism. Meanwhile, zein nanoparticles loaded with PHL were successfully prepared using the anti-solvent precipitation method, which was evidenced by the morphology and size characterization. The hydrogen bond and hydrophobic interaction in the nanoparticles were further confirmed by Fourier transform infrared spectroscopy. This study elucidates the noncovalent interaction mechanism between zein and PHL, providing a theoretical foundation for the design of zein-polyphenol nanocarriers. These carriers show promising applications as emulsion stabilizers or delivery systems for lipophilic bioactives, thereby facilitating the development of functional foods with improved stability and enhanced bioavailability.

Received 18th November 2025
Accepted 27th January 2026

DOI: 10.1039/d5ra08898d

rsc.li/rsc-advances

1. Introduction

Phloretin (PHL), a flavonoid featuring a distinctive dihydrochalcone structure, is abundant in apples and apple-derived products. It boasts remarkable attributes, including potent whitening, antibacterial, antioxidant, and anti-inflammatory benefits[1] with safety and reliability well-established in the food industry. Despite these advantages, PHL's notoriously poor solubility and limited bioavailability significantly constrain its commercial application. Encouragingly, a recent study reveals that encapsulating phloretin within a nanostructured lipid carrier can dramatically boost its bioavailability.[2] Furthermore, earlier studies demonstrated that forming an inclusion complex with hydroxypropyl-β-cyclodextrin significantly enhances PHL's water solubility.[3]

Growing interest surrounds the application of protein-derived biopolymer nanoparticles for adsorbing and encapsulating hydrophobic substances. Protein-based polymers are highly preferred over synthetic alternatives owing to their outstanding biocompatibility, greenness, and utility.[4] Among these, zein stands out as the principal storage protein in maize, distinguished by its amphiphilic nature.[5] Classified as Generally Recognized as Safe (GRAS) by the Food and Drug Administration (FDA).[6] Zein nanoparticles readily self-assemble *via* anti-solvent precipitation (ASP) technology. Transforming zein into nanoparticles offers significant advantages, including exceptionally mild preparation conditions, strong potential for large-scale industrial production, remarkable biocompatibility, and biodegradability,[7] and its ideal role as an embedding form and highly suitable carrier material for loading and transporting hydrophobic compounds.[4]

A widely adopted approach to functionalize protein-based carriers involves the formation of non-covalent complexes with polyphenolic compounds.[8] Such interactions can improve the stability of the carrier system, fine-tune release profiles, and introduce supplementary bioactivities. Protein-polyphenol binding is inherently complex and requires comprehensive characterization using complementary analytical techniques.[9,10]

Previous studies on the zein-polyphenol system have begun to reveal this complexity. Some authors observed that the influence of varying concentrations of $CaCl_2$ exhibited a more pronounced effect on the interaction between zein and FA when compared to analogous effects observed with KCl, NaCl, and $MgCl_2$.[11,12] Yue *et al.* investigated how zein and isoquercetin

[a]*State Key Laboratory of Marine Food Processing and Safety Control, National Engineering Research Center of Seafood, School of Food Science and Technology, Dalian Polytechnic University, Dalian 116034, China. E-mail: foodscixiaodong@dlpu.edu.cn; qinningbo6902765@163.com*

[b]*Liaoning Key Lab of Lignocellulose Chemistry and Biomaterials, Liaoning Collaborative Innovation Center for Lignocellulosic Biorefinery, School of Light Industry and Chemical Engineering, Dalian Polytechnic University, Dalian 116034, China*

[c]*Department of Food Science and Nutrition, The Hong Kong Polytechnic University, Hom Hung, Kowloon, Hong Kong, China*

(ISO) interact and the structural changes involved.[13] They found that hydrogen bonds and van der Waals forces are the main contributors to this interaction. Moreover, the existence of hydrophobic interaction was also noted.

Zein has been extensively used to load and encapsulate some small-molecule hydrophobic substances, including but not limited to curcumin, quercetin, ISO, epigallocatechin-3-gallate (EGCG), and FA.[11,13–16] Nevertheless, the utilization of zein nanoparticles for the encapsulation of PHL has not yet been investigated. At the molecular and physicochemical levels, the mechanism of interaction between zein and PHL requires further elucidation.

Therefore, we aimed to decipher the mechanism and structural alterations between zein and PHL by means of a combination of analytical techniques, including fluorescence spectra, UV-vis, and circular dichroism (CD) spectra. The binding sites of PHL and zein were predicted by the molecular docking method, and the thermodynamic parameters and force types were determined. Meanwhile, zein nanoparticles loaded with PHL (ZPNPs) were successfully prepared and characterized *via* ASP method. This study offers valuable reference information and a solid theoretical basis for designing and developing effective zein-based carriers for broadening the application of hydrophobic polyphenols such as PHL in food industry.

2. Experimental

2.1. Chemicals and reagents

Zein and phloretin (purity >98%) were purchased from Aladdin Chemical Co., Ltd (Shanghai, China).

2.2. Preparation of zein-PHL complex solutions

Zein and PHL powders were accurately weighed and dissolved in a 70% (v/v) ethanol solution to make a 1 mM zein solution and a 10 mM PHL solution. Various volumes of PHL solution were combined to produce a series of zein-PHL complex solutions. Finally, the concentration of zein was established at 10 μM, while the concentrations of PHL ranged from 0 to 25 μM, with specific concentrations designated as 0, 5, 10, 15, 20, and 25 μM, respectively.

2.3. Preparation of zein nanoparticles loaded with PHL

This method is analogous to earlier research methods, with minor modifications.[13] Zein and PHL were added to a 70% (v/v) aqueous ethanol solution in mass ratios of 10 : 1, at a zein concentration of 10 mg mL^{-1}. Afterward, the zein-PHL stock solution mixture was stirred magnetically at 600 rpm for an hour.

The ZPNPs were formed by adding the zein-PHL stock solution into deionized water (zein-PHL stock solution to deionized water in a volume ratio of 4 : 1), during which the ZPNPs underwent continuous magnetic stirring at 600 rpm for half an hour. Ethanol was subsequently eliminated using a rotary evaporator set at 40 °C and −0.1 MPa. The amount of ethanol lost was compensated with deionized water to get a nanoparticle dispersion solution. The precipitate was then removed by centrifugation for 20 min at 4000 rpm. The PHL-loaded composite nanoparticles were named ZPNPs.

2.4. UV-visible absorption spectroscopy

As previously outlined by Yang *et al.*, 3 mL of zein-PHL complex solution was transferred into a cuvette and subsequently scanned within the 250–450 nm range by means of a UV-vis spectrophotometer (UV-2550, Shimadzu, Japan).[17] Prior to scanning, 70% (v/v) ethanol solution was employed for baseline correction.

2.5. Fluorescence spectroscopy analysis

2.5.1. Fluorescence spectroscopy determination. A fluorescence spectrophotometer (F-7000, Hitachi, Japan) was used to determine the fluorescence spectra of zein-PHL complex solutions. The samples were prepared in a water bath at different temperatures (298 K, 308 K, and 318 K), and the protein concentration was fixed at 10 μmol L^{-1}.[18] The parameters of the scanning program are outlined below: an excitation wavelength of 280 nm, an emission wavelength ranging from 290 to 450 nm, a scanning speed of 1500 nm min^{-1}, and an excitation and emission slit width of 5.0 nm.

2.5.2. Analysis of fluorescence quenching types. Dynamic quenching results from the collision of a fluorophore with a quenching agent, in contrast to static quenching, which occurs when a stable complex is formed between them. The distinction between these two quenching types is determined by their respective excited state lifetimes and disparate responses to temperature.[19] The Stern–Volmer equation was utilized to analyze the type of fluorescence quenching of zein by PHL.[20] The following formula was employed:

$$F_0/F = 1 + K_{sv}C_q = 1 + K_q\tau_0C_q \quad (1)$$

where F_0 and F represent the florescence intensity values of zein before and after the addition of PHL, respectively, K_{sv} was the quenching constant, K_q denoted the quenching reaction rate constant, C_q is the concentration of PHL, and τ_0 was the lifetime of the fluorescent molecule of zein in the absence of a quenching agent, with a value of 10^{-8} s.

2.5.3. Binding constants and binding sites. The binding constants and number of binding sites for the static quenching mechanism were calculated based on the double logarithmic Stern–Volmer equation, which is given below.[21]

$$\log((F_0 - F)/F) = \log K_a + n\log C_q \quad (2)$$

where K_a is the binding constant, and n is the number of binding sites.

2.5.4. Thermodynamic parameters. The thermodynamic parameters in the process of zein combining with PHL were calculated using the Van't Hoff and thermodynamic principles, and the interaction force between PHL and zein was analyzed.[22]

$$\ln K_a = -\Delta H/RT + \Delta S/R \quad (3)$$

$$\Delta G = \Delta H + T\Delta S \quad (4)$$

where the free energy change (ΔG), entropy change (ΔS), and enthalpy change (ΔH) represent the thermodynamic parameters of the binding process, while K_a is the binding constant, T is the experimental temperature (K), and R is the gas constant (8.314 J (mol K)$^{-1}$).

2.6. Circular dichroism spectra determination (CD)

The CD spectra of the zein-PHL complex solutions were measured using a CD spectrometer (J1500, Jasco, Tokyo, Japan), with the zein concentration maintained at 10 μM and the instrument set to scan from 190 to 260 nm. The molar ellipticity was derived by acquiring each spectrum and performing a subtraction of the baseline calibration.

2.7. Molecular docking

Zein (ID: Q41844) was selected from the UniProt database for molecular docking with PHL (CID: 4788), which was retrieved from PubChem. The original structures of both were processed using DeepMice (http://www.deepmice.com/). The results obtained after docking were repaired by PLIP (Protein–Ligand Interaction Profiler) and then analyzed and visualized by PyMOL software to better understand the interaction mode of PHL molecules (ligand) and zein (receptor). The binding energy of them was predicted by using Dockeasy. Discovery Studio was used to analyze the mode of interaction between zein and PHL.

2.8. Determination of particle size, polydispersity index (PDI), and zeta potential

The average particle size, PDI, and zeta-potential of nanoparticles were evaluated using dynamic light scattering (DLS) (Nano-ZS90, Malvern Instruments, Worcestershire, UK) at 25 °C. The DTS1070 model was utilized as the measuring container for the loading of the sample. These samples were equilibrated for 120 s at 25 °C and repeated three times.

2.9. Scanning electron microscopy (SEM)

Fresh nanodisperse droplets were placed on a small round piece of glass, dried, gold-coated, and scanned with SEM (JSM-7800F, JEOL, Japan) at magnifications of 50 000× to observe changes in nanoparticle microstructure.

2.10. Surface hydrophobicity measurement

According to the established protocols, ANS was used as the fluorescent probe, and the fluorescence spectrometer (F-7000, Hitachi, Tokyo, Japan) was employed to assess the effect of PHL on the hydrophobicity of zein protein surface.[23] ANS fluorescence spectra were captured across 400–600 nm under standardized conditions: 5.0 nm excitation slit width, 2.5 nm emission slit width, and 390 nm excitation wavelength. Surface hydrophobicity of zein-PHL complexes was quantified through relative ANS fluorescence intensity analysis.

2.11. Fourier transform infrared spectroscopy (FTIR) and X-ray diffraction (XRD)

The sample solution was stored in a refrigerated environment at −20 °C and freeze-dried for two days. Mix the freeze-dried samples with the potassium bromide in a sufficient amount using an agate mortar and pestle. After drying and pressing the prepared samples, FTIR spectra were subsequently obtained using an FTIR spectrometer (SpectrumTwo, PerkinElmer, Japan). XRD analysis of zein, PHL, and ZPNPs was conducted with an X-ray diffractometer (XRD-6100S, Shimadzu, Japan), scanning across a 2θ range of 5–70° under an accelerating voltage of 40 kV and a current of 30 mA.

2.12. Differential scanning calorimetry (DSC) and thermogravimetric (TGA)

DSC and TGA were tested using a differential scanning calorimeter (DSC Q2000, TA Instruments, USA) and a thermogravimetric analyzer (TGA 550, TA Instruments, USA). Samples weighing approximately 3.0 mg were heated at a rate of 20 °C min^{-1} in an open porcelain crucible with nitrogen gas flow, within a temperature range of 25–300 °C.

2.13. Statistical analysis

Each experiment was triplicated, and data were expressed as the mean ± standard deviation. Statistical analysis was conducted using SPSS 20 to evaluate differences among experimental samples, with significance set at $p < 0.05$. Images were generated using Origin 2021.

3. Results and discussion

3.1. Effect of PHL on UV-vis spectroscopy of zein

The application of ultraviolet-visible spectroscopy is beneficial for understanding protein-small molecule interactions.[24] When a small molecule binds to a protein, the absorption spectrum of the protein is altered, which is reflected by an amplified or reduced signal.

Due to the susceptibility of 200–220 nm UV absorption to solvent effects, the 250–450 nm UV absorption spectra of single PHL solution, single zein solution, and zein-PHL solution were determined. From Fig. 1A, PHL has an absorption peak at 286 nm due to its conjugated structure. From Fig. 1B, a single zein solution has a UV absorption peak around 277 nm because of the conjugated structure of its aromatic amino acid residues. The zein absorbance around 277 nm exhibited a significant increase following PHL, a phenomenon that may be attributed to the entry of PHL between the hydrophobic amino acid residues of zein. The phenolic hydroxyl group of phloretin can form hydrogen bonds with amino acid residues of zein, and its hydrophobic domain binds to the hydrophobic region of the protein, causing protein conformational changes and enhancing UV absorption intensity, suggesting an interaction between zein and PHL.

Furthermore, as the concentration of added PHL gradually increased, the spectral characteristics of zein underwent significant changes, specifically manifested as the peak shifting

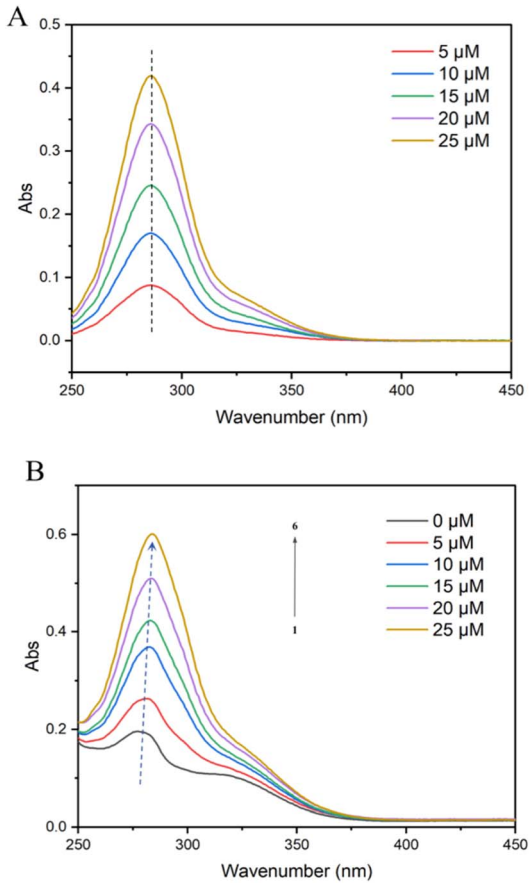

Fig. 1 UV absorption spectra of PHL solution (A) and zein-PHL mixture solution (B).

to the wavelength of 284 nm. This shift can be attributed to intermolecular interactions that altered the microenvironment of the chromophore from nonpolar to polar, resulting in a redshift of the absorption spectrum. This phenomenon is exactly as reported by Zhao *et al.* in the case of the zein – EGCG system. With the increase of EGCG concentration, the absorbance of zein obviously increases, while the maximum absorption wavelength do not change.[20] The magnitude of the redshift further supports a binding mechanism dominated by hydrophobic interactions and cavity encapsulation rather than superficial adsorption.

3.2. Analysis of fluorescence spectra and quenching types

The fluorescence quenching technique identifies the specific binding between proteins and small molecules. It measures the attenuation of fluorescence intensity to reveal the affinity of the binding site and analyzes molecular interactions.[25] The fluorescence spectra of the complex were measured at temperatures of 298, 308, and 318 K, and it was found that they exhibited similar patterns (Fig. 2A–C). As the PHL content rises, the fluorescence intensity of zein diminishes, typically due to the quenching effect of small-molecule substances like polyphenols on the aromatic amino acids in proteins.[26] This phenomenon is indicative of an interaction between PHL and zein.

As shown in Fig. 2D and Table 1, further clarification of the mechanism of PHL inducing fluorescence quenching according to the Stern–Volmer curves. These curves exhibited clear linear relationships at 298, 308, and 318 K. K_q significantly exceeded the limiting diffusion collision quenching constant (2.0×10^{10} L (mol s)$^{-1}$).[8] Consequently, the quenching mechanism of PHL on zein was primarily governed by static quenching. Quenching parameters K_{sv} progressively increased with rising temperature, which indicates that there may be a large hydrophobic interaction in the quenching process, because the hydrophobic interaction tends to be enhanced with the increase of temperature. Therefore, it can be inferred that the hydrophobic interaction plays an important role in the formation of the zein-PHL complex.

3.3. Binding constant and number of binding sites

From Fig. 2E, the logarithmic curves of zein and PHL at different temperature conditions were obtained. It can be observed that the linear relationship is good, indicating that K_a and n were obtained reliably and efficiently. As shown in Table 1, the K_a for zein and PHL decreased as the temperature increased. As shown in Table 1, the K_a between zein and PHL decreased with rising temperature, indicating a weakening of their interaction. This trend aligns thermodynamically with $\Delta H < 0$, confirming the binding to be exothermic—heat is released upon complex formation. Consequently, increasing temperature shifts the equilibrium toward dissociation, thereby reducing K_a. Furthermore, $\Delta S < 0$ supports this mechanism, reflecting an increase in structural order upon binding. This indicates that the binding force between them weakens at higher temperatures, negatively impacting their stability and interaction strength. This underscores the importance of maintaining optimal temperatures for effective binding and interaction between zein and PHL. Additionally, it has been observed that both zein and PHL possess at least one binding site, and the interaction between zein and PHL molecules has been confirmed.

3.4. Thermodynamic analysis

The main types of interactions between molecules were analyzed by thermodynamic parameters. The thermodynamic parameters ΔH and ΔS between zein and PHL, as shown in Table 1, are less than zero, indicating that the primary interaction forces at play are hydrogen bonding and van der Waals forces. This phenomenon is remarkably similar to the interaction forces observed between whey protein isolates and anthocyanins.[27] Since $\Delta G < 0$ supports the notion that the interaction between zein and PHL occurs spontaneously. This spontaneous interaction is similar to that previously reported between curcumin and zein.[28]

3.5. CD spectra and secondary structure analysis

CD spectra serve as a robust analytical tool capable of capturing critical secondary structure information for proteins within the 190 to 260 nm range, thereby enabling a detailed investigation into PHL's effect on zein conformational changes. As clearly

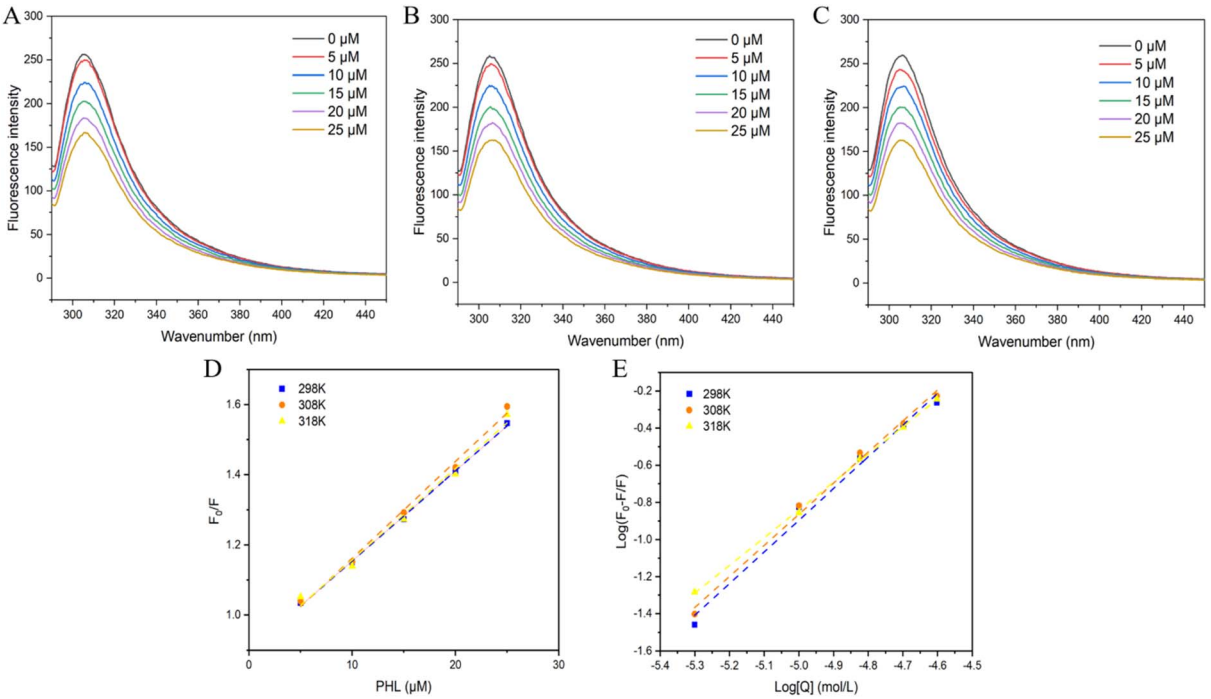

Fig. 2 Effect of PHL on the fluorescence intensity of zein at different temperatures: 298 K (A), 308 K (B), 318 K (C). Stern–Volmer plot of F_0/F as a function of PHL concentration at different temperatures (D) and plot of $\log[(F_0 - F)/F]$ as a function of log of PHL concentration (E) in the zein-PHL mixtures at different temperatures. F_0 and F represent the fluorescence intensity in the absence and presence of PHL, respectively.

exhibited in Fig. 3A, both the position and intensity of the characteristic peaks at 195 nm and 208 nm underwent significant alterations. These results further substantiate that PHL exerted a certain influence on the secondary structure of the zein-PHL complex, ultimately triggering changes within its microenvironment following PHL addition. A diagram outlining the analyzed secondary structure content is presented in Fig. 3B.

When the level of PHL increased (0–30 μM), the relative content of α-helix of the zein-PHL complex increased from 34.6% to 39.3%, whereas that of β-sheet decreased from 18.6% to 13.3%. Hydrogen bonds are the main driving force that maintains the α-helix structure in proteins.[29]

Since the concentration of PHL increases, the original hydrogen bonds break, and new hydrogen bonds replace some of the original intermolecular hydrogen bonds. The decrease in β-sheet content is attributed to PHL, which triggers the hydrophobic interaction between PHL and zein, thereby disrupting the β-sheet structure. Significant alterations were observed in the α-helix and β-sheet, whereas the β-turn and random coil contents did not exhibit major changes. This might result from PHL binding to proteins, which causes the protein molecules' hydrogen bonds to flip.[30] In this study, the observed increase in α-helix content aligns with previous findings on zein–phenol interactions. Yue *et al.* reported that the α-helix content of zein increased from 36.07% to 42.21% upon binding with isoquercitrin (ISO), reaching 45.41% at higher concentrations.[13] Similarly, Zhu *et al.* observed an increase from 56.4% to 58.7% in the α-helix content of zein after interaction with rutin, with a maximum of 59.4%.[31] This structural stabilization is

Table 1 Quenching parameters (K_{sv} and K_q), binding constant (K_a), and binding sites of zein-PHL complexes (n) for the zein/PHL system reaction at different temperatures, and thermodynamic parameters of interaction between zein-PHL complexes. The results in the table represents the means ± SDs ($n = 3$)

		T (K)		
		298	308	318
Quenching parameters	K_{sv} (10^4 L mol^{-1})	2.143	2.363	2.376
	K_q (10^{12} L (mol s)$^{-1}$)	2.143	2.363	2.376
Binding constants and binding sites	N	1.707	1.674	1.493
	K_a (L mol^{-1})	4.363×10^7	3.231×10^7	4.201×10^6
Thermodynamic parameters	ΔG (KJ mol^{-1})	−44.310	−42.729	−41.148
	ΔH (KJ mol^{-1})	−91.421		
	ΔS (J (mol K)$^{-1}$)	−158.091		

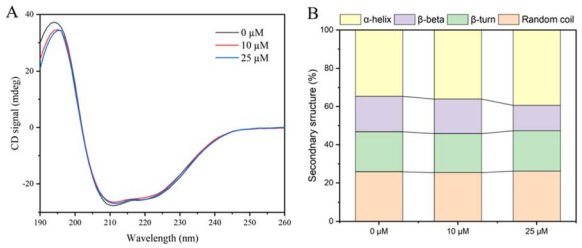

Fig. 3 CD spectra (A) and secondary structure content (B) of zein-PHL. The PHL concentrations are 0, 10, and 25 μmol L^{-1}.

attributed to an intermolecular hydrogen-bond network formed between PHL's phenolic hydroxyl groups and the zein backbone. The result is further corroborated by thermodynamic data: the result is further corroborated by thermodynamic data: hydrogen-bond formation releases energy ($\Delta H < 0$) and increases structural order ($\Delta S < 0$), corresponding to the rise in α-helix content. These outcomes reveal that an increase in PHL concentration led to hydrophobic interactions and hydrogen bonding within the zein-PHL complex, resulting in distinct spatial conformational modifications. This implies a change in the microenvironment's polarity, leading to the conformation change of zein. The results are consistent with the ultraviolet spectrum and fluorescence spectrum.

3.6. Molecular docking of PHL with zein

The structural changes of zein and PHL during the binding process were described through molecular docking. The crystal structure of zein was obtained from the Uniprot Data Bank [ID: Q41844]. The three-dimensional (3D) structure is shown in Fig. 4A. A 3D structure for PHL (CID: 4788) from PubChem is shown in Fig. 4B.

Dockeasy was used to store the docking results, and the binding energy between zein and PHL was −27.94 kJ mol^{-1}. The stability of intermolecular bonding is higher with lower binding energy, leading to more energy being released during complex formation. Fig. 4C shows the binding site of PHL in the 3D structure of zein. The amino acid residues THR206, ASN209, GLN173, GLN216, GLN219, LEU205, TYR213, and ALA212 create a cavity in which PHL is securely bound. A closer examination reveals that the specific arrangement and interactions of these amino acid residues contribute significantly to the stability of the cavity. Among them, the hydrophobic side chains of LEU205 and ALA212 form a dense core structure with the aromatic ring of TYR213, which effectively repels water molecules and thus enhances the binding ability of PHL. In addition, polar residues THR206, ASN209, GLN173, GLN216, and GLN219 further stabilize the complex structure through hydrogen bonding. This sophisticated interaction network ensures that PHL remains stable within the binding cavity, fully highlighting the important role of these residues for the overall stability and function of the protein. Further analysis reveals that several interactions occur between PHL and the surrounding amino acids, including hydrophobic interactions, van der Waals forces, and hydrogen bonding. These molecular interactions are fundamental to the structural stability of the complex, and their mechanism of action corresponds to the non-covalent interactions observed between EGCG and zein.[32]

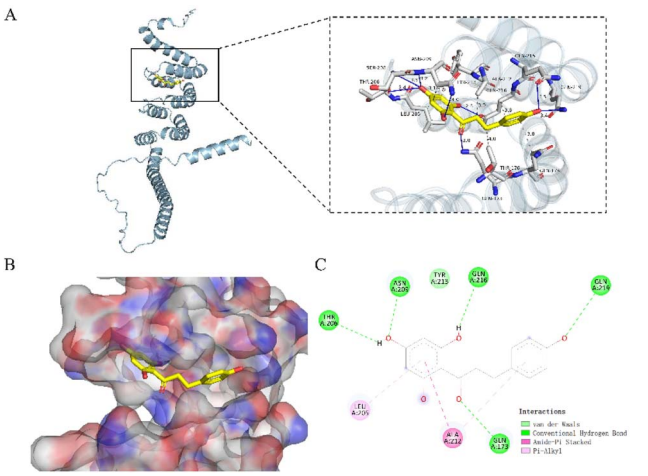

Fig. 4 Three-dimensional structure mode of zein-PHL complexes (A); surface structure of PHL in the hydrophobic pocket inside zein (B); binding site of PHL and zein (C).

In typical protein-polyphenol interactions, the binding free energy (ΔG) serves as a key indicator of complex stability and functional potential. The weak non-covalent complexes typically exhibit binding energies higher than −20 kJ mol^{-1}, while strong specific binding is less than −30 kJ mol^{-1}. Here, the binding energy between zein and PHL, determined *via* molecular docking, was measured at −27.94 kJ mol^{-1}, which falls within the moderately strong range. The obtained value thus indicates that the zein–PHL complex possesses considerable structural stability, consistent with the behavior of many functional protein–polyphenol systems.

Collectively, the results of molecular docking experiments provide evidence that zein can utilize its cavity structure to encapsulate PHL, and this encapsulation mechanism not only ensures a tight fit but also significantly enhances the stability of PHL, further reinforcing the reliability of this molecular interaction.

3.7. Formation and characterization of ZPNPs

3.7.1. Particle size, PDI, and zeta potential. The particle size distribution diagram and potential distribution diagram of ZPNPs are shown in Fig. 5A. The average particle size of PHL-zein nanoparticles prepared by anti-solvent precipitation method was 77.04 ± 1.42 nm, with a PDI value of 0.294 ± 0.03. The zeta potential value was 24.63 ± 6.38 mV (Fig. 5B). Studies show that the particle size is affected by the formula composition and preparation method. The lower the zein concentration, the higher the ethanol content, and the faster the stirring speed, the smaller the particle size of the prepared nanoparticles.[33,34] In the process of anti-solvent preparation, with the decrease of ethanol concentration in the solution, zein self-assembled from the loose state to form solid spherical particles, and embedded phloretin inside the zein nanoparticles through hydrogen

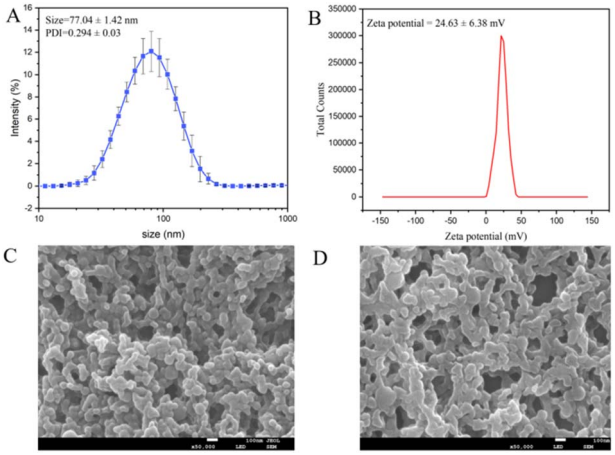

Fig. 5 The particle size and PDI (A), zeta-potential (B) of nanoparticles, and SEM of zein (C) and ZPNPs (D).

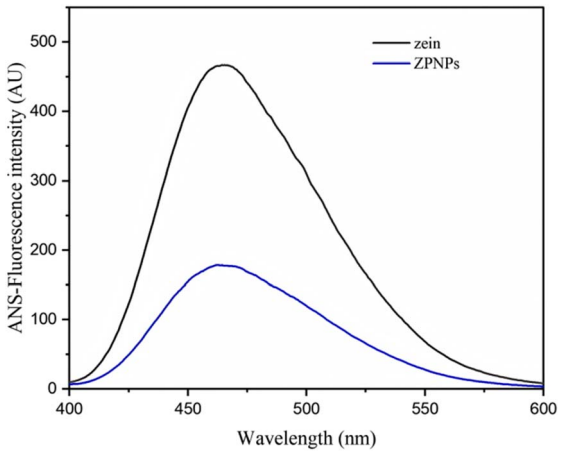

Fig. 6 The ANS-fluorescence spectra of zein and ZPNPs.

bonding, van der Waals force, hydrophobic interaction, and other driving forces.

3.7.2. SEM analysis. SEM revealed that zein nanoparticles, with or without PHL loading, underwent significant aggregation and adhesion upon drying (Fig. 5C and D). This phenomenon primarily stems from capillary forces during the drying process, yet it also reflects a strong inherent adhesion tendency of the particle surfaces, driven by hydrophobic interactions. Notably, the incorporation of PHL did not induce noticeable morphological alterations to the nanoparticles. This observation aligns with and corroborates the thermodynamic data ($\Delta H < 0$, $\Delta S < 0$), indicating that PHL binds to the hydrophobic regions of zein proteins *via* hydrogen bonding and van der Waals forces. This interaction facilitates the encapsulation of PHL within the nanoparticle matrix during self-assembly, rather than mere surface adsorption. Thus, the structural evidence confirms that PHL exists as a stable complex within the nanoparticles, laying a foundational basis for its subsequent functional performance.

3.7.3. ANS-fluorescence spectra and surface hydrophobicity analysis. Alterations in protein conformation can be manifested as shifts in surface hydrophobicity, a property that influences protein interactions and functionality. ANS, a hydrophobic fluorescent probe, specifically targets and binds to exposed hydrophobic patches on the protein surface. This interaction triggers a notable increase in fluorescence intensity, providing a measure of surface hydrophobicity.[35] The ANS-fluorescence spectrum of ZPNPs was recorded and presented in Fig. 6.

The experimental results showed that the addition of PHL reduces the hydrophobicity of the zein surface. This trend was in perfect alignment with the previously surfaced hydrophobicity values for zein and resveratrol.[36] This phenomenon can be attributed to the specific binding interaction between PHL and the zein-ANS system. When PHL binds to this system, it effectively obstructs the hydrophobic domains on the protein's surface. This blockade leads to a significant reduction in the overall surface hydrophobicity of zein nanoparticles.[35]

3.7.4. FTIR analysis. FTIR spectroscopy stands out as one of the most widely utilized methods for the identification and detailed characterization of the structural composition of various compounds. Assessing the nature of non-covalent interactions that occur between PHL and zein by this technique (Fig. 7A). The findings derived from this analysis revealed that all spectra of samples consistently exhibit a broad band spanning the range of 3100 to 3600 cm^{-1}, a phenomenon that is unequivocally attributed to the stretching vibrations characteristic of the O–H bond.[37] The characteristic peak associated with the –OH group in zein manifests at a wavelength of 3335 cm^{-1}, whereas the broadband corresponding to PHL is observed at 3264 cm^{-1}. However, a significant shift is evident in the spectra of ZPNPs, where the distinctive peak of the –OH group migrates to 3317 cm^{-1}, providing compelling evidence of the formation of hydrogen bonds between PHL and zein.[38]

Additionally, the typical absorption peaks of zein, which are prominently located at 1660 and 1531 cm^{-1}, are intricately linked to the amide I band, representing the stretching

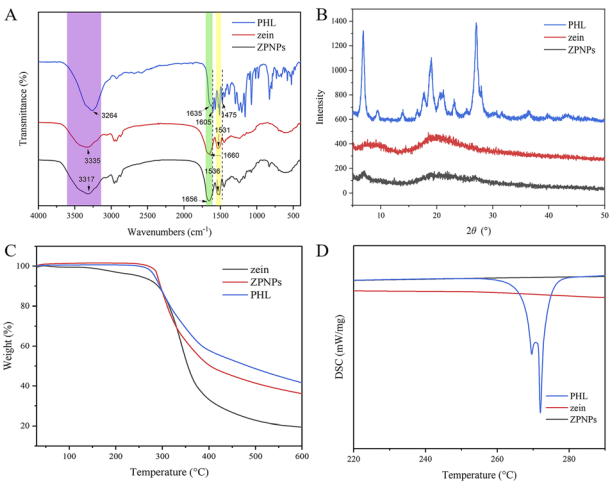

Fig. 7 Infrared spectra (A), XRD patterns (B), TGA (C), and DSC (D) curve plot of PHL, zein, and ZPNPs samples.

vibrations of the C=O bond, and the amide II band, which is associated with the combined stretching and bending vibrations of the C–N and N–H groups, respectively.[39] In the context of ZPNPs, the peak of the amide I band undergoes a subtle shift to 1656 cm^{-1} when compared to the spectrum of pure zein, while the amide II band experiencesa corresponding shift to 1536 cm^{-1}. These shifts are ascribed to the presence of hydrogen bonding that arises among the molecular components of zein and PHL.[37] Furthermore, the characteristic absorbance bands of PHL, notably at 1605 and 1475 cm^{-1}, are associated with the distribution of benzene rings. The characteristic sharp peaks of crystalline PHL are diminished in the ZPNPs spectrum, a process facilitated by hydrophobic interactions.[40]

Overall, FTIR provides robust confirmation that PHL has been successfully encapsulated within zein nanoparticles. The intricate network of interactions, including hydrogen bonding and hydrophobic effects, collectively constitute the primary driving forces that facilitate the assembly and stabilization of the zein-PHL composite nanoparticles.

3.7.5. XRD analysis. Powerful insights into the physical state of nanoparticles are offered by X-ray diffraction analysis, a technique for elucidating the structural characteristics of materials[38] (Fig. 7B). The diffraction pattern of zein revealed two broad peaks at 9.58° and 20.24°, which are characteristic of an amorphous structure. In stark contrast, PHL displayed a series of sharp diffraction peaks spanning the range from 5° to 50°. These sharp peaks are indicative of a highly crystalline nature. However, a notable transformation was observed in the ZPNPs. The distinct crystallization peaks that were prominently present in the PHL sample nearly disappeared in the ZPNPs. This significant change implies that PHL underwent a transition from a crystalline to an amorphous state. Such a transition is likely due to the intermolecular interactions between zein and PHL, which disrupt the ordered crystalline structure of PHL. This disruption results in a more disordered, amorphous arrangement of the PHL molecules within the nanoparticles. The near absence of crystallization peaks in the ZPNPs further suggests that PHL was effectively incorporated into the nanoparticles.

3.7.6. TGA and DSC analysis. Fig. 7C meticulously illustrates the TGA curves for zein, PHL, and ZPNPs. The temperature range was monitored between 25 and 250 °C. It was observed that only zein lost 5% of its mass within this range. This was primarily attributable to the evaporation of residual water molecules. This first stage of mass loss is a common phenomenon of thermal analysis, showing the removal of moisture from the samples. At the elevated temperature of 600 °C, the mass loss rates for zein, PHL, and ZPNPs were recorded as 80.5%, 58.4%, and 63.8%, respectively. These figures provide a quantitative measure of the thermal degradation behavior of each component, highlighting the relative stability of the composite nanoparticles compared to their individual constituents. These data indicate that the incorporation of composite nanoparticles has the potential to significantly enhance the thermal stability of zein, at least to a certain, appreciable extent. This enhancement is crucial for applications requiring materials that can withstand high temperatures without significant degradation.

The DSC curve plots for zein, PHL, and ZPNPs are depicted in Fig. 7D. The melting of PHL crystals resulted in the formation of a distinct endothermic peak at 269.6 °C and 272 °C, providing unequivocal evidence that PHL is indeed a crystalline substance. This characteristic endothermic peak is a hallmark of crystalline materials undergoing phase transition from solid to liquid.

Notably, the typical DSC profiles for ZPNPs did not exhibit any endothermic peak corresponding to PHL, a particularly intriguing finding. This absence suggests that PHL and zein have formed an amorphous complex within the nanoparticle structure. This amorphous complex effectively hinders the crystallization of PHL under the constraints imposed by the nanoparticles, thereby altering its thermal behavior. This phenomenon is supported by Sun *et al.*,[41] who delves into the interactions between zein and dihydromyricetin at the molecular level.

The DSC results are in perfect harmony with the findings from prior XRD investigations. These complementary analyses collectively demonstrate that PHL was not only encapsulated within the zein matrix but also remained in an amorphous state, thereby confirming the successful formation of a stable composite material.

4. Conclusion

In the present study, molecular docking studies revealed that the zein cavity encapsulated PHL. The predominant interaction mechanisms between PHL and zein are primarily hydrogen bonds and van der Waals forces, along with some hydrophobic interactions. This discovery is in line with the experimental data. Furthermore, the zein nanoparticle was formulated using the anti-solvent precipitation process. While this work provides a fundamental basis for developing PHL-loaded active carriers, a key limitation remains: the inherent hydrophobicity of zein nanoparticles leads to aggregation in aqueous dispersion, limiting their colloidal stability and practical applicability. To effectively address and mitigate this challenge, various strategies can be employed. The use of surfactants or polysaccharides can play a pivotal role in modifying, coating, and stabilizing these nanoparticles. By implementing these changes, not only is the stability of the nanoparticles significantly enhanced, but their loading capacity is also notably improved. Future work should further evaluate the performance of these optimized carriers under simulated food processing conditions—including thermal, pH, and ionic stress—as well as assess their long-term storage stability and bioavailability. These steps are essential for advancing zein-based PHL delivery systems toward functional food and nutraceutical applications.

Author contributions

Siyang Chen: conceptualization, data curation, investigation, methodology, visualization, writing—original draft. Jinhui Jia: conceptualization, investigation. Jian Du: supervision,

validation. Ningbo Qin: supervision, validation, writing—review and editing. Xiaodong Xia: conceptualization, funding acquisition, writing—review and editing.

Conflicts of interest

The relevant work of this article does not involve financial interest disputes without competition.

Data availability

The data that support the findings of this study are available from the corresponding author upon reasonable request.

Acknowledgements

This work was supported in part by the National Key Research and Development Program of China (2022YFD2100104), Liaoning Innovation Consortia Major Project (2023JH1/11200001), Basic Scientific Research Funds of Universities in Liaoning Province (LJBKY2024042) and National Natural Science Foundation of China (32472350).

References

1 S. Chen, W. Zhu, Y. Zhan and X. Xia, *Foods*, 2024, **13**, 3537.
2 L. Gu, R. Sun, W. Wang and Q. Xia, *Chem. Phys. Lipids*, 2022, **242**, 105150.
3 Y. Wei, J. Zhang, A. H. Memon and H. Liang, *J. Mol. Liq.*, 2017, **236**, 68–75.
4 S. Chen, Q. Li, D. J. McClements, Y. Han, L. Dai, L. Mao and Y. Gao, *Food Hydrocolloids*, 2020, **99**, 105334.
5 C. Liu, B. Xu, D. J. McClements, X. Xu, S. Cui, L. Gao, L. Zhou, L. Xiong, Q. Sun and L. Dai, *Food Chem.*, 2022, **391**, 133224.
6 A. C. Jaski, F. Schmitz, R. P. Horta, L. Cadorin, B. J. G. da Silva, J. Andreaus, M. C. D. Paes, I. C. Riegel-Vidotti and L. M. Zimmermann, *Ind. Crops Prod.*, 2022, **186**, 115250.
7 M. Lin, S. Fang, X. Zhao, X. Liang and D. Wu, *Food Hydrocolloids*, 2020, **106**, 105871.
8 C. Tan, J. Zhu, C. Shi, X. Zhang, S. Lu, S. Wang, C. Guo, C. Ning and Y. Xue, *Food Chem.*, 2025, **464**, 141586.
9 Q. Yuan, L. He, X. Wang, H. Yang, F. Zhu, X. Peng, J. Cheng, Y. Lin, D. Tang and X. Liu, *Food Hydrocolloids*, 2024, **149**, 109522.
10 K. Horita, T. Kameda, H. Suga and A. Hirano, *Food Res. Int.*, 2025, **202**, 115573.
11 Q. Wang, Y. Tang, Y. Yang, L. Lei, X. Lei, J. Zhao, Y. Zhang, L. Li, Q. Wang and J. Ming, *Food Hydrocolloids*, 2022, **124**, 107251.
12 Q. Wang, Y. Tang, Y. Yang, L. Lei, X. Lei, J. Zhao, Y. Zhang, L. Li, Q. Wang and J. Ming, *Food Chem.*, 2022, **373**, 131489.
13 X. J. Yue, P. W. Xu, X. C. Luo and B. Zhao, *Int. J. Biol. Macromol.*, 2024, **263**, 130412.
14 Z. Zhang, Y. Hu, H. Ji, Q. Lin, X. Li, S. Sang, D. Julian McClements, L. Chen, J. Long, A. Jiao, X. Xu, Z. Jin and C. Qiu, *Food Chem.*, 2023, **415**, 135736.
15 C. Z. Liu, N. Lv, G. R. Ren, R. B. Wu, B. J. Wang, Z. X. Cao and H. J. Xie, *Food Hydrocolloids*, 2021, **120**, 106906.
16 X. Zhang, Y. Lu, R. Zhao, C. Wang, C. Wang and T. Zhang, *Food Hydrocolloids*, 2022, **124**, 107331.
17 T. Yang, G. Tao, L. Li and Q. Ma, *J. Food Eng.*, 2023, **359**, 111700.
18 X. Wang, X. Li, J. Xue, H. Zhang, F. Wang and J. Liu, *Food Chem.:X*, 2022, **16**, 100454.
19 Z. Allahdad, A. Khammari, L. Karami, A. Ghasemi, V. A. Sirotkin, T. Haertlé and A. A. Saboury, *Food Hydrocolloids*, 2020, **108**, 106003.
20 S. Zhao, W. Wang, R. Zhao, T. Yan, W. Xu, E. Xu and D. Liu, *LWT–Food Sci. Technol.*, 2022, **170**, 114110.
21 Z. Zang, S. Chou, J. Tian, Y. Lang, Y. Shen, X. Ran, N. Gao and B. Li, *Food Chem.*, 2021, **336**, 127700.
22 Y. Wang, S. Wang, X. Zhang, W. Wu, W. Bai and L. Tian, *Food Hydrocolloids*, 2024, **154**, 110125.
23 M. Deshpande and S. K. Sathe, *J. Food Sci.*, 2018, **83**, 1847–1855.
24 Z. Wu, J. Xu, J. Ruan, J. Chen, X. Li, Y. Yu, X. Xie, J. Tang, D. Zhang and H. Li, *Food Chem.:X*, 2023, **18**, 100734.
25 C. Li, T. Dai, J. Chen, X. Li, T. Li, C. Liu and D. J. McClements, *Food Chem.*, 2021, **339**, 128145.
26 S. Parolia, J. Maley, R. Sammynaiken, R. Green, M. Nickerson and S. Ghosh, *Food Chem.*, 2022, **367**, 130603.
27 S. Ren and M. M. Giusti, *Foods*, 2021, **10**, 310.
28 P. Tiwari, R. Ali, R. Ishrat and N. Arfin, *J. Mol. Struct.*, 2021, **1230**, 129637.
29 Y. Wang, P. Zhang, H. Lin, X. Fei, G. Zhang and X. Hu, *Food Hydrocolloids*, 2024, **154**, 110084.
30 Q. Liu, Y. Li, Y. Zhou, L. Jiang, Q. Lyu, G. Liu, X. Wang, X. Chen and L. Chen, *Food Chem.*, 2022, **387**, 132926.
31 J. Zhu, Z. Li, C. Wu, G. Fan, T. Li, D. Shen, J. Dou and Y. Liang, *Food Chem.*, 2023, **404**, 134684.
32 E. P. Vale, W. de S. Tavares, Z. Hafidi, L. Pérez, M. del C. Morán, M. Martin-Pastor and F. F. O. de Sousa, *J. Mol. Liq.*, 2024, **394**, 123718.
33 X. Huang, X. Huang, Y. Gong, H. Xiao, D. J. McClements and K. Hu, *Food Res. Int.*, 2016, **87**, 1–9.
34 G. Davidov-Pardo, I. J. Joye and D. J. McClements, *Food Hydrocolloids*, 2015, **45**, 309–316.
35 R. Li, L. Huang, Z. Zhang, J. Chen and H. Tang, *Food Chem.*, 2022, **386**, 132839.
36 T. Dai, R. Li, C. Liu, W. Liu, T. Li, J. Chen, M. Kharat and D. J. McClements, *Food Hydrocolloids*, 2019, **97**, 105234.
37 H. Liang, B. Zhou, L. He, Y. An, L. Lin, Y. Li, S. Liu, Y. Chen and B. Li, *R. Soc. Chem. Adv.*, 2015, **5**, 13891–13900.
38 X. Wang, M. Li, F. Liu, F. Peng, F. Li, X. Lou, Y. Jin, J. Wang and H. Xu, *Food Chem.*, 2021, **364**, 130335.
39 J. Y. Shi, W. Q. Cai, X. T. Luo, B. L. Su, J. W. Xiao, G. R. Zhang, Q. Q. Yang and B. B. Zhang, *Biochem. Eng. J.*, 2023, **197**, 108992.
40 M. P. Kapoor, M. Moriwaki, M. Ozeki and D. Timm, *Carbohydr. Polym. Technol. Appl.*, 2021, **2**, 100046.
41 C. C. Sun, H. Su, G. D. Zheng, W. J. Wang, E. Yuan and Q. F. Zhang, *Food Chem.*, 2020, **330**, 127245.